Journal of Porous Materials (2021) 28:1215–1225
https://doi.org/10.1007/s10934-021-01068-2

PVP-assisted Sn-Ti microspheres for the efficient B–V oxidation of cyclohexanone

Chuanfa Liu[1] · Zhiwei Zhou[1] · Juan Qin[2] · Guangbo Xia[1] · Yangyang Liu[1] · Binbin He[1] · Fanqing Li[1] · Peiyong Sun[3] · Wenliang Wu[1]

Published online: 5 April 2021

Abstract

New Sn-Ti microspheres were first successfully synthesized by a PVP-assisted sol-gel method in this paper, and their performance in the B–V oxidation of cyclohexanone was investigated. The XRD, N_2 sorption, SEM, Py-IR, UV–Vis, XPS, EDX, Elemental mapping and TEM characterization techniques were utilized to investigate their physical and chemical properties. Based on the proposal possible formation mechanism, in the MTS-x sample synthesis procedure, the introduction of PVP as a stabilizer and dispersant can coordinate the hydrolysis rate of two different precursors resulting in the hindrance of their agglomerations. And the HDA as a precipitation accelerator and morphology control agent can be beneficial to the formation of spheres by increasing the hydrogen-bonding interactions. The MTS-12 as well as the weight percent of tin to titanium species of 12 with specific regular microspheres has the highest cyclohexanone conversion of 97.8% and the highest ε-caprolactone selectivity of 98.2%, which is better than the bulk Sn-TiO_2 catalyst even though that the weight percent of tin to titanium species was 18. The catalysts with higher accessible active sites and shorter diffusion channels would provide a valuable theoretic reference for the industrial process of the B–V oxidation of cyclohexanone for the preparation of caprolactone.

Keywords Sn-Ti microspheres · PVP · HDA · Cyclohexanone · *E*-Caprolactone

1 Introduction

ε-Caprolactone is a new type of polyester monomer. Owing to the reason that its polyester has good biocompatibility and biodegradability, it is widely used in biomedical engineering, degradable plastic and high value-added packaging materials [1–3]. Traditionally, ε-caprolactone is mainly produced by cyclohexanone Baeyer–Villiger (B–V) oxidation with organic peroxyacid as the oxidant [4]. But organic peroxyacid has tremendous hidden danger during transportation and storage, and a large amount of waste acid is generated during the reaction, which is easy to cause environmental pollution. Therefore, it is urgent to seek for other oxidants to replace them [2, 5]. At present, there are two main methods used to prepare ε-caprolactone [6, 7]. The first one is the hydrogen peroxide as the oxidant [8, 9]. The other is the benzaldehyde/O_2 method, also known as the Mukaiyama method [10, 11]. The former has weak oxidation capacity when the hydrogen peroxide concentration is too low, and it is easy to explode when the concentration is high [12]. At the same time, water will be generated during the reaction resulting in the hydrolysis of ε-caprolactone, which is not conductive to industrial process [13]. The benzaldehyde/O_2 method will be quite attractive owing to the fact that it is well matched to both environmental and cost concerns [14–16]. Up to now, many materials such as hydrotalcite [17], zeolite (molecular sieve) [18], carbon materials [19], composite metal oxides [20] and mesoporous oxides [21] have been used as catalysts in the cyclohexanone B–V

✉ Zhiwei Zhou
zhiweizhou@njtech.edu.cn

✉ Wenliang Wu
wwl@njtech.edu.cn

[1] College of Chemical Engineering, Nanjing Tech University, Nanjing 210009, People's Republic of China

[2] Technology and Finance Service Center of Jiangsu Province, Productivity Center of Jiangsu Province, Nanjing 210042, People's Republic of China

[3] School of Chemical Engineering, Beijing Institute of Petrochemical Technology, Beijing 100012, People's Republic of China

oxidation reaction. It is an inspired catalyst preparation strategy to introduce Sn^{4+} into zeolite (molecular sieve) or mesoporous metal oxide to improve the Lewis acidity and activate the carbonyl group of cyclohexanone, thereby promoting the cyclohexanone B–V oxidation. For example, Sn-beta zeolite [22], Sn-MCM-41 [23], Sn-SBA-15 [24] and Sn-SBA-16 [25] have all been proved to be a good class of catalysts. In our previous reports, we successfully incorporated Sn^{4+} into Al_2O_3 and TiO_2 framework by an evaporation induced self-assembly method (EISA) to form the specific mesoporous Sn-Al_2O_3 [26]and Sn-TiO_2 [27, 28], and they showed good catalytic performance in the cyclohexanone B–V oxidation with molecular oxygen.

Spherical mesoporous materials (SMMs), especially TiO_2 microspheres, are of great interests owing to the unique and regular spherical shape, which showed the closed packing nature and lowest surface energy. The open mesopores and short channels of SMMs not only increase the density of high accessible active sites but also facilitate the mass diffusion with short length [29]. Until now, many methods have been developed to prepare TiO_2 microspheres, including sol-gel method [30, 31], hydrothermal or solvothermal synthesis method [32, 33], templates method [34, 35] and spray method [36, 37]. Among them, the sol-gel method is a better method because of its simple preparation procedure and the characteristics of toward controlled synthesis [38]. However, only pure TiO_2 microspheres can be prepared by traditional sol-gel method. Other species would difficultly be incorporated into the TiO_2 microspheres because of the different atomic or ionic structural sizes and valence states, which would cause the various hydrolysis rates resulting in the destruction of the spherical shape during the preparation process. Therefore, some other specified substances would be introduced to make the same hydrolysis rate of different species. PVP (Polyvinylpyrrolidone) is widely used as an effective surfactant to control the morphology during the synthesized process [39]. In the preparation procedure, PVP can be physically adsorbed on the surface of the polymer as a stabilizer and dispersant to prevent the polymer from agglomerating with each other [40] because of the strong steric hindrance with the five membered ring side groups in its molecular structure. On the other hand, since both the similar ion radius and equal valence state of Sn^{4+} (0.069 nm) and Ti^{4+} (0.061 nm), tin species can be easily incorporated into the skeleton of TiO_2 microspheres by a PVP-assisted sol-gel method. The Sn-doped TiO_2 microspheres combining Lewis acidity resulting from the incorporation of tin species and the advantages of microspheres are expected to achieve the desired results in cyclohexanone B–V oxidation reaction, and no relative literatures on this work have been reported.

In this paper, a series of mesoporous MTS-x catalysts were synthesized by a PVP-assisted sol–gel method. The characterization of XRD, N_2 sorption, SEM, Py-IR, UV–Vis, XPS, EDX, Elemental mapping and TEM were utilized to investigate their physical chemical properties. Furthermore, the catalytic performance was investigated in the cyclohexanone B–V oxidation, and the catalyst formation and catalytic mechanisms were also clarified.

2 Experimental

2.1 Preparation of catalysts

All the chemicals were of analytical grade and were used without further purification. In a typical synthesis procedure [41], 1.5 g of hexadecylamine (HDA) was added to the reactor with 200 mL of ethanol and 1.3 mL of H_2O, and then vigorously stirred for 30 min to obtain a uniform solution A. Tetrabutyl titanate (3.4 mL) and tin tetrachloride (0, 0.035 g, 0.105 g, 0.175 g, 0.245 g, 0.315 g) were dissolved in ethanol (10 mL) under stirring. Then 0.3 g of polyvinylpyrrolidone (PVP) was slowly added to obtain solution B. After that, solution B was quickly added to solution A, and the stirring speed was immediately turned down to 500 rpm for 5 min. After aging for 24 h, the white precipitate was harvested by centrifugation, and then washed three times with ethanol to remove residual HDA, and then dried at 80 °C for 12 h. For the heat treatment, the samples were annealed at 400 °C for 3 h with a heating rate of 2 °C min^{-1}. The as-prepared samples were abbreviated as MTS-x, in which MTS and x refer to mesoporous Sn–Ti microspheres and the weight percent of tin to titanium species, respectively.

2.2 Characterization of catalysts

The XRD patterns of the catalysts were obtained on a Bruker D8 instrument with Ni-filtered Cu Kα radiation (λ = 0.154 nm) and operated at 40 kV and 100 mA. The scanning range was from 10 to 80° for the wide-angle X-ray diffraction patterns. UV–Vis DRS for the catalysts were measured on Lambda 950 spectrophotometer. The wavelength range was from 200 to 800 nm and the $BaSO_4$ was as a reference compound. The surface chemical composition was analyzed by XPS on the Thermo Scientific Escalab 250 Xi spectrometer with Al Kα X-ray source (1486 eV). FT-IR spectra of pyridine (Py-IR) were obtained on the Thermo Nicolet Nexus spectrometer in KBr pellets. The catalysts was pretreated in 10^{-2} Pa at 573 K for 3 h and then cooled down to room temperature. After that, pyridine was adsorbed for 2 h and the temperature was raise to 473 K for 1 h to remove the physisorbed pyridine. N_2 sorption isotherms were measured at 77 K using a BELSORP-MINI volumetric adsorption analyzer. The samples were degassed at 473 K for 3 h under vacuum before measurement. The BET method and BJH adsorption model were used for calculating surface area and

determining pore size distribution, respectively. The morphology of the catalyst was observed by S4800 scanning electron microscope (SEM). The dispersion of elements on the surface of the material was detected by the energy scanning electron microscope of Oxford INCA EDAX. The dispersion of the semi-quantitative elemental composition was measured by energy dispersive X-ray (EDX) spectrometer in the Oxford INCA EDAX Detecting Unit. The morphology of the catalysts was visualized using JEOL JEM-2010 EX transmission electron microscope (TEM) under 200 kV after the samples were dispersed in ethanol assisted by an ultrasonic technique.

2.3 Catalytic test

The catalytic performance of the synthesized catalysts were investigated in the B–V oxidation of cyclohexanone by molecular oxygen, which was carried out in a three neck flat bottom flask equipped with a reflux condenser at atmospheric pressure. In a typical process, 0.24 g catalyst and 2.4 g benzaldehyde as pro-oxygenic agent were simultaneously added into the solution containing of 1 g cyclohexanone and 30 g acetonitrile as solvent. The solution was raised up to 343 K and molecular oxygen was introduced to the reaction system at a rate of 10 mL/min. After that, it was kept for 5 h with continuous stirring. After that, the flask was cooled down to room temperature and the reaction mixture was analyzed on a SP-6890 gas chromatograph equipped with a SE-30 column (0.25 μm × 50 m) and a flame ionization detector (FID). The cyclohexanone conversion and ε-caprolactone selectivity were calculated when dodecane was the internal standard. The reuse ability of the catalyst was investigated by filtration without any treatment in the recycling tests.

3 Results and discussion

3.1 Catalyst characterization

Figure 1 shows SEM images of MTS-x catalysts. As shown in Fig. 1, compared to the sample d, sample g prepared without PVP showed irregular particles, indicating that the PVP is essential to the formation of microspheres. For sample a, few microspheres with partial surface defect were obtained. With the mass ratio of tin species to titanium species increasing from 0 to 12, more and more regular microspheres with uniform size would be obviously observed, suggesting the incorporated tin species would not destroy the structures. However, when the mass ratio of tin species to titanium species further increased, the microspheres would be broken and they would be agglomerated, which may be owing to the and fact that excessive tin species broke the equilibrium of condensation between titanium and tin complexes, resulting in the destruction of spheres.

Figure 2 shows XRD patterns of MTS-x catalysts. It can be seen from Fig. 2 that the diffraction peaks of the catalyst a~d were ascribed to anatase phase of TiO_2 (JCPDS No. 21-1272) [42], where the peak intensities would be promoted with the increase of tin species. However, when the mass ratio of tin to titanium species was exceeded to 12, a characteristic diffraction peak of rutile phase at around $2\theta = 27.4°$ can be obviously appeared [43], which may be attributed to the reason that crystal transformation during calcination would happen by the excessive amount of tin species resulting in the peak intensities decreasing [44]. No characteristic diffraction peaks of SnO_2 or other Sn_xTiO_y species in all catalysts were observed, which may

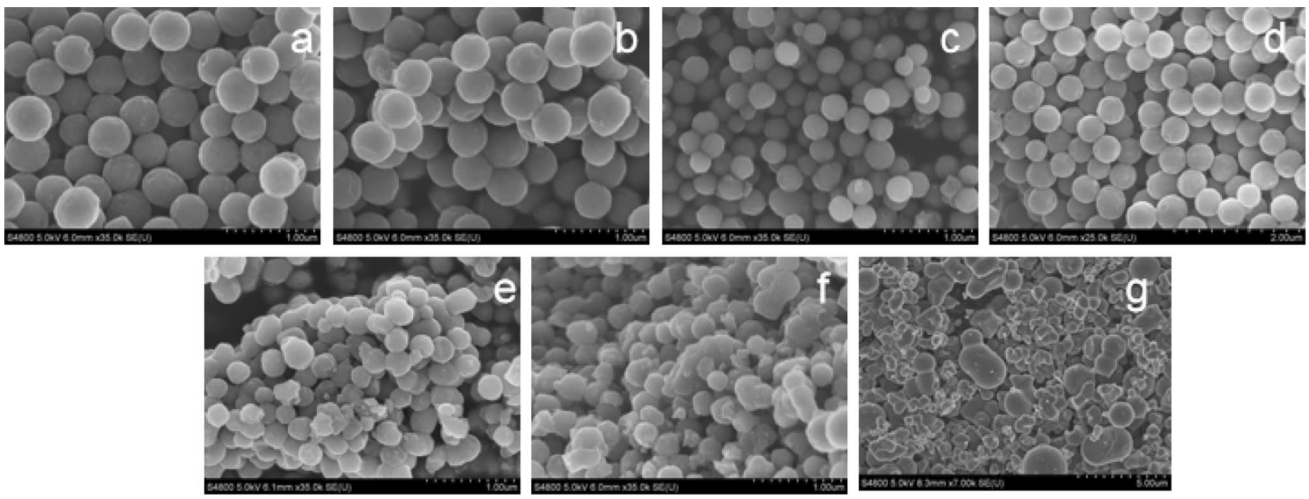

Fig. 1 SEM images of MTS-x catalysts. (a) MTS-0, (b) MTS-2.4, (c) MTS-7.2, (d) MTS-12, (e) MTS-16.8, (f) MTS-21.6, (g) MTS-12 without PVP

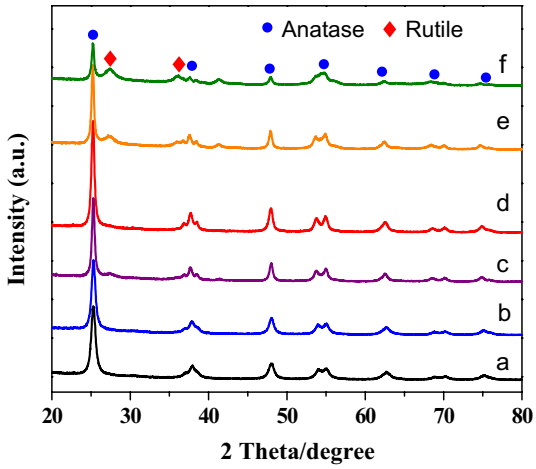

Fig. 2 XRD patterns of MTS-x catalysts. (a) MTS-0, (b) MTS-2.4, (c) MTS-7.2, (d) MTS-12, (e) MTS-16.8, (f) MTS-21.6

be due to the fact that tin species were highly dispersed or homogeneously incorporated into the framework of mesoporous TiO_2 microspheres [45].

Figure 3 shows N_2 sorption isotherms and pore size distribution curves of MTS-x catalysts. As can be seen form Fig. 3a that all the isotherms show type-IV adsorption-desorption isotherms along with a H2 hysteresis loop, which is due to the capillary condensation of N_2 in the mesopores, indicating that all the catalysts are typical mesoporous structures [46]. At the same time, the hysteresis loop would be promoted with the tin species increasing, which may be owing to the reason that tin species can be successfully incorporated into the framework of mesoporous TiO_2 resulting in the increase of pore volume. It can be seen from Fig. 3b, only a sharp peak around 3.7 nm can be observed for all the catalysts, indicating their mesoporous size was uniform. Some physical properties were listed in Table 1. With the increase of tin species, the specific surface area and pore volume of the catalyst increased, which also indicated that tin species were successfully incorporated into TiO_2 microspheres [47]. However, compared to the MTS-0 sample, the pore size of tin-doped TiO_2 microspheres was almost unchanged owing to the almost equal diameter between Sn^{4+} and Ti^{4+} probably. In addition, the mass ratio of tin to titanium species for all the MTS-x samples is almost equal to the initial feed ratio, suggesting all the tin species can be incorporated into the framework.

Figure 4 shows Py-IR curves of MTS-x catalysts. The absorption peak at 1450 cm^{-1} corresponds to the interaction between the Lewis acid and pyridine molecule [48]. It can be obtained from Figure 4 that the Lewis acidity would be promoted by the incorporation of tin species when the weight percentage of Sn/Ti was below 21.6, and it increased with the tin species loadings increasing, which would activate carbonyl groups in the molecular structure of cyclohexanone resulting in the improvement of catalytic performance. However, as the Sn/Ti weight percentage reached 21.6, the Lewis acidity of MTS-21.6 catalyst decreased sharply, which may be ascribed the MTS-21.6 catalyst had a large amount of rutile phase leading to reduction in the amount of tin incorporated into the framework [28].

Figure 5 shows UV–Vis DRS patterns of (a) MTS-0 and (b) MTS-12. It can be seen from the Fig. 5 that the absorption of both samples was below 400 nm. For MTS-12, a new peak centered 210 nm corresponding to the tetrahedral coordinated tin species can be observed, further suggesting their successful incorporation [49]. Compared with MTS-12, the

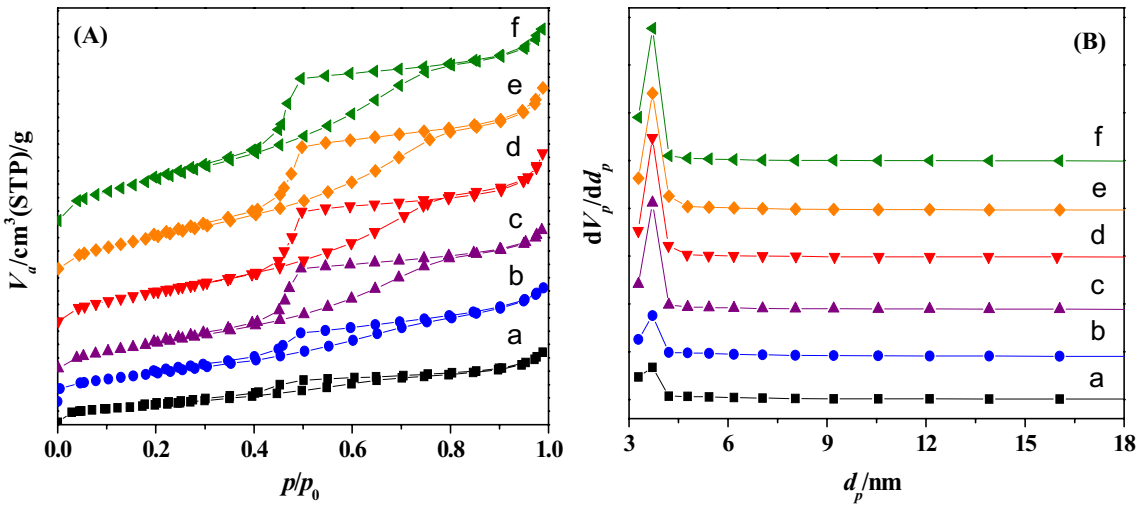

Fig. 3 N_2 sorption isotherms and pore size distribution curves of MTS-x catalysts. (a) MTS-0, (b) MTS-2.4, (c) MTS-7.2, (d) MTS-12, (e) MTS-16.8, (f) MTS-21.6

Table 1 Physical properties for MTS-x catalysts

Catalysts	Pore size/(nm)[a]	$S_{BET}/(m^2 \cdot g^{-1})$[b]	Pore volume/$(cm^3 \cdot g^{-1})$[c]	Sn/Ti[d]
MTS-0	3.71	14.53	0.04	0.0
MTS-2.4	3.72	22.53	0.05	2.6
MTS-7.2	3.72	31.39	0.08	7.0
MTS-12	3.72	38.39	0.10	11.6
MTS-16.8	3.72	39.20	0.11	17.3
MTS-21.6	3.72	46.44	0.12	21.0

[a]Barrett-Joyner-Halenda method

[b]Brunner–Emmet–Teller specific areas

[c]$P/P_0 = 0.9$

[d]EDX analysis

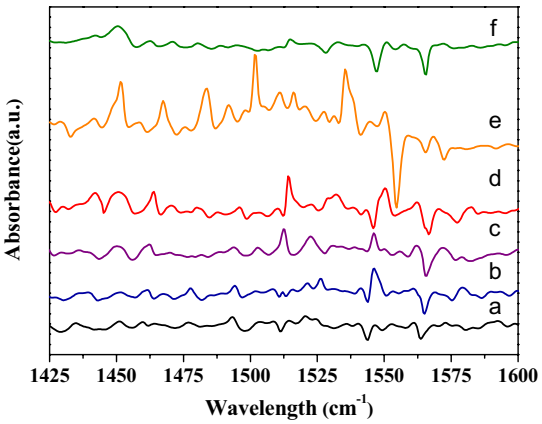

Fig. 4 Py-IR curves of MTS-x catalysts. (a) MTS-0, (b) MTS-2.4, (c) MTS-7.2, (d) MTS-12, (e) MTS-16.8, (f) MTS-21.6

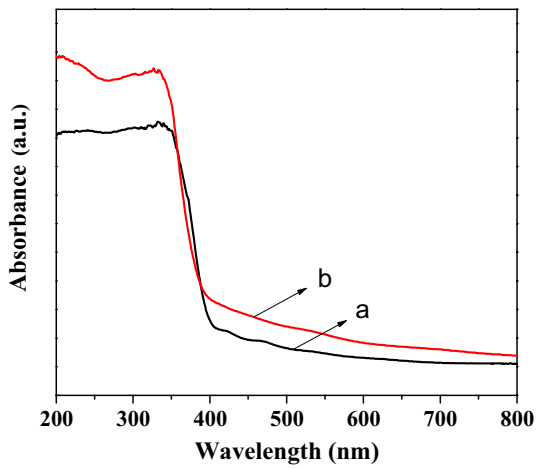

Fig. 5 UV–Vis DRS patterns of (a) MTS-0 and (b) MTS-12 samples

maximum absorption peak of MTS-0 shifts slightly to the right, which probably owing to the decreased crystallinity based on the XRD patterns [50]. For MTS-12, there was no obvious peak at the 400 nm center band, indicating that no bulk SnO_2 was obtained in the MTS-12 catalyst [49], which was consistent with XRD characterization.

Figure 6 shows XPS spectra of (a) MTS-0 and (b) MTS-12 samples. It can be seen from Fig. 6a the strong peak at 529.8 eV can be ascribed to Ti-O [51], and the tailing peak at 531.9 eV may be owing to the -OH group absorbed on the surface [52]. Figure 6b shows the XPS spectra of the Sn 3d region. The peaks at 486.1 eV and 495.5 eV are ascribed to Sn $3d_{5/2}$ and Sn $3d_{3/2}$, which can be concluded that the Sn^{4+} species can be formed in the lattice [53]. Compared to MTS-0 sample, a positive shift of Ti 2p and O 1s energy peaks for the MTS-12 sample can be observed because of the interactions between Ti, O and Sn species resulting in the formation of Ti-O-Sn framework [54]. At the same time, the Ti 2p peaks with binding energy of 458.7 eV and 464.5 eV, corresponding to Ti $2p_{3/2}$ and Ti $2p_{1/2}$, respectively, can be observed in Fig. 6c, further suggesting their successful tetrahedral coordination [55].

Figure 7a shows elemental mapping pictures of MTS-12 sample. It can be seen from Fig. 7a that the X-ray signal distributions of Ti, Sn and O elements were all spherical indicating that all the three elements are homogenously dispersed in the sample, which can further demonstrated that tin species were successfully incorporated into the TiO_2 microspheres. Figure 7b and c shows TEM images of MTS-12 sample. It can be seen that the microsphere diameter about 450 nm and the lighter contrast along the edge compared to the center can be observed, suggesting the short-ranged pores would facilitate the diffusion of the substrates [56].

3.2 Catalytic performances

The catalytic performances for the MTS-x catalysts in the B–V oxidation of cyclohexanone by molecular oxygen are listed Table 2. From entry 1, no cyclohexanone conversion was obtained suggesting that the benzaldehyde was indispensable as an oxygen promoter. In Entry 2, the cyclohexanone conversion of 36.2% and the ε-caprolactone selectivity of 81.9%, respectively, can be formed in the absence of catalyst. Cyclohexanone conversion was 80.2% and ε-caprolactone selectivity was 83.6% from Entry 3 when the MTS-0 as catalyst, which is much higher than our previous literatures [27, 28] owing to the superiority of the formation of microspheres. At the same time, the cyclohexanone conversion and the ε-caprolactone selectivity would be improved with the weight percent of tin to titanium species increasing from 0 to 12. And the highest cyclohexanone conversion of 97.8% and ε-caprolactone selectivity of 98.2% over MTS-12 catalyst in Entry 6 can be reached, which is much higher than the

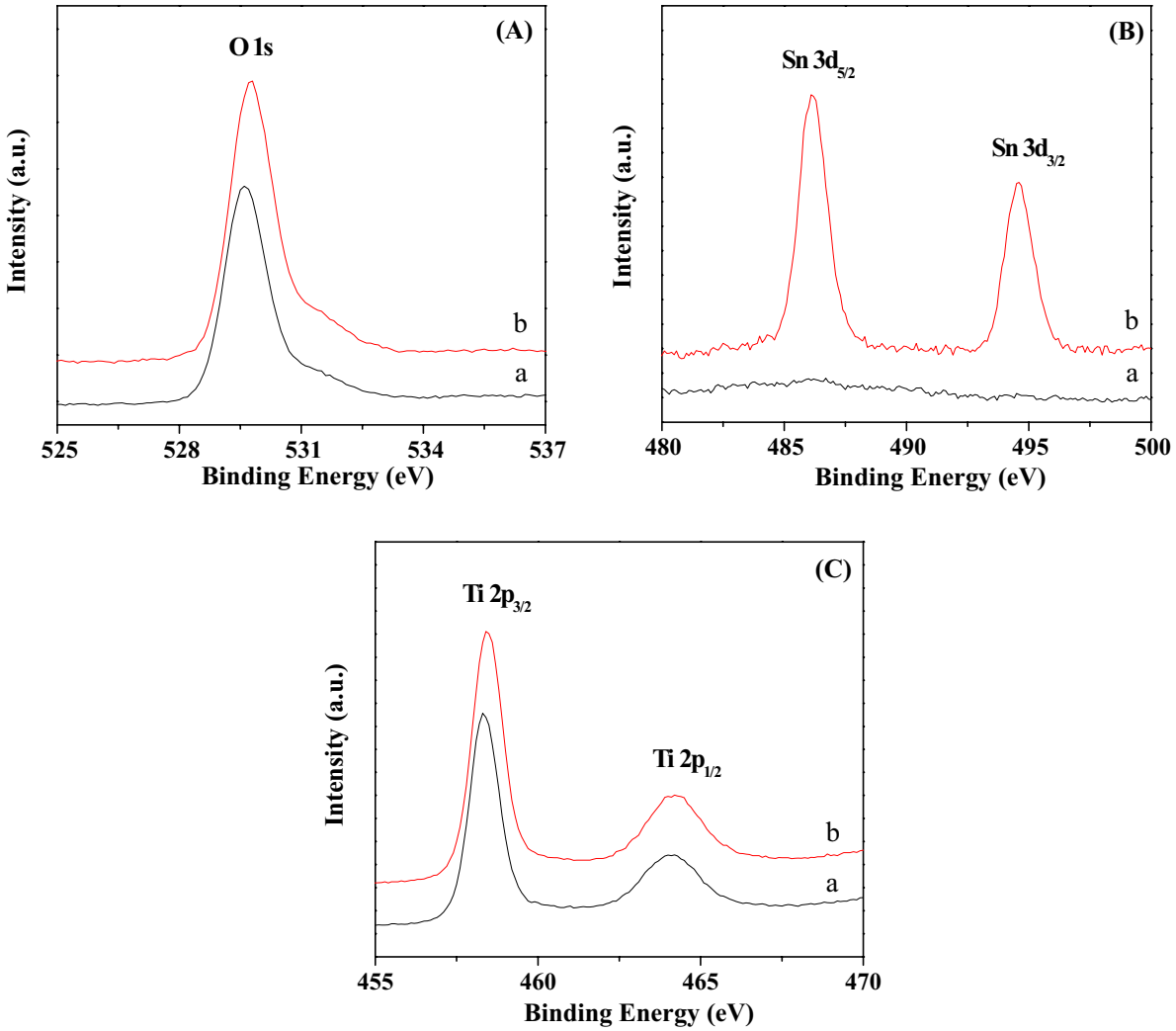

Fig. 6 XPS spectra of (a) MTS-0 and (b) MTS-12 samples

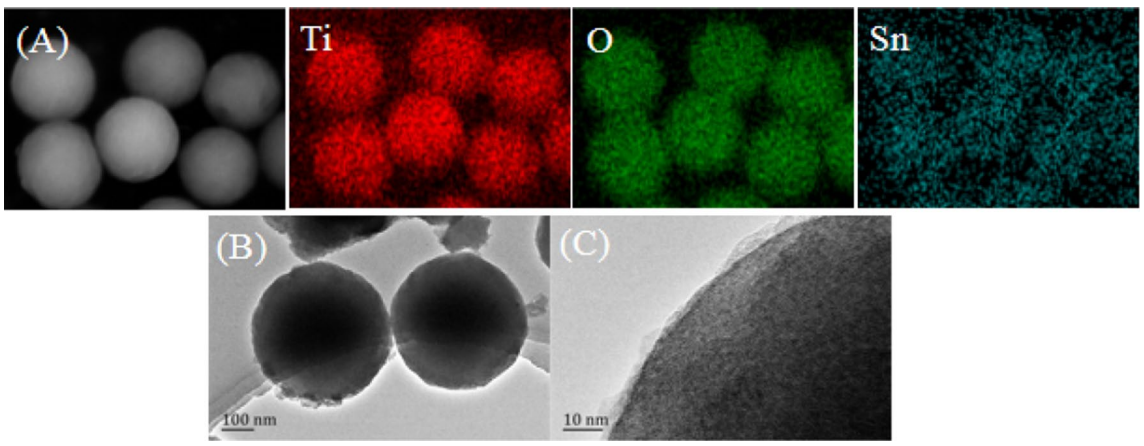

Fig. 7 Elemental mapping pictures and TEM images of MTS-12 sample

Table 2 Catalytic performances for MTS-x in the B-V oxidation of cyclohexanone

Entry	Catalysts	Cyclohexanone conversion/%	ε-Caprolactone selectivity/%	ε-Caprolactone yield/%
1[a]	MTS-12	–	–	0
2	None	36.2	81.9	29.6
3	MTS-0	80.2	83.6	67.1
4	MTS-2.4	83.8	87.4	73.2
5	MTS-7.2	90.1	92.5	83.3
6	MTS-12	97.8	98.2	96.0
7	MTS-16.8	93.6	94.7	88.6
8	MTS-21.6	89.9	88.1	79.2
9[b]	MTS-12	95.2	96.2	91.6

Reaction conditions: w (cyclohexanone) /w (catalyst) /w (acetonitrile) /w (benzaldehyde) = 1/0.24/30/2.4; reaction time: 5 h; reaction temperature: 70 °C.

[a]In the absence of benzaldehyde

[b]w (cyclohexanone) /w (catalyst) /w (acetonitrile) /w (benzaldehyde) = 1/0.24/30/2.2; reaction time: 5 h; reaction temperature: 70 °C

catalytic performance of bulk 12Sn-TiO_2 and 12Sn-TiO_2-EN catalysts based on our previous reports [27, 28]. It can interestingly found that although the tin species loading is lower than 18Sn-TiO_2-EN catalyst, the catalytic performance over MTS-12 is much higher in Entry 9. It may be owing to the reason that the unique mesoporous microspheres not only increased the density of active sites, but also shortened the diffusion path of the substrates than bulk ones. In addition, although the highest Lewis acidity for MTS-16.8 catalyst was obtained, the catalytic performance would be dropped because of the microspheres aggregations probably. Further increasing the tin species loading, cyclohexanone conversion and cyclohexanone conversion would further decreased owing to the formation of some rutile phase resulting in the microspheres destruction.

To test the heterogeneity of MTS-12 catalyst, leaching experiments were carried out according to previous reports [57, 58]. The catalyst was removed at 1 h under the optimal reaction condition by hot filtration. Then, the filtrate was applied for further reaction under the same reaction condition. The results of leaching experiment are shown in Figure 8. It can be seen that the conversion of cyclohexanone at 1 h (before catalyst removal) was 65.4%. With the increasing of reaction time, a slight enhancement in cyclohexanone conversion was observed, which may be attribute to the little leached tin species dispersed on the support surface through the hydrogen bonding rather than incorporated tin species in the matrix of mesoporous TiO_2 microsphere. The chemical composition of the fresh and filtered catalysts was also analyzed by XRF techniques. Compared to the fresh catalyst, the tin content for the filtered catalyst slightly decreased

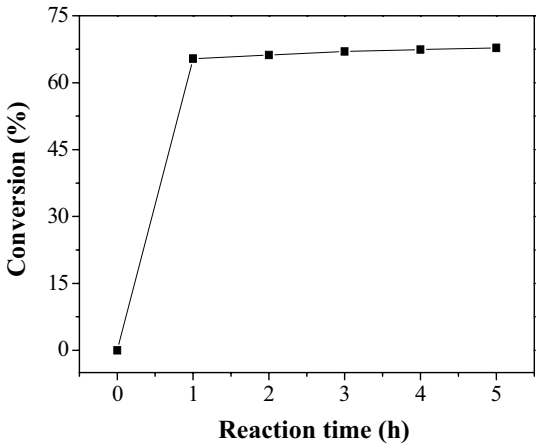

Fig. 8 Leaching experiment of MTS-12 catalyst in the B-V oxidation of cyclohexanone with molecular oxygen. Reaction conditions: w (cyclohexanone)/w (catalyst)/w(acetonitrile)/w(benzaldehyde) = 1/0.24/30/2.4; reaction time: 5 h; reaction temperature: 70 °C

from 11.7 to 11.5 wt.%, which indicated that the tin species incorporated in the MTS-12 sample was stable and thereby resistant to leaching.

Figure 9 shows the catalytic stabilities for MTS-12 catalyst in the B–V oxidation of cyclohexanone. As can be seen from Fig. 9, the cyclohexanone conversion and ε-caprolactone selectivity of MTS-12 catalyst slightly decreased with increase of the recycle number. The ε-caprolactone yield of MTS-12 catalyst dropped from 96.0 % to 82.4% after repeated use for 5 times, which proved the good stability of the MTS catalyst.

In addition, the catalytic performance between MTS-12 and other reported tin-based catalysts was compared, and the results were listed in Table 3. It can be seen that

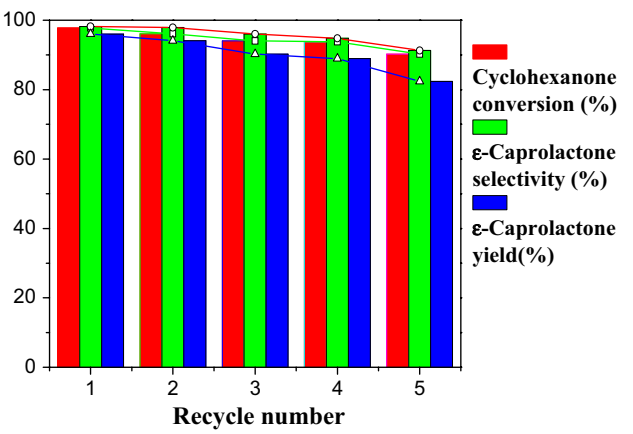

Fig. 9 Catalytic stabilities for MTS-12 catalyst in the B-V oxidation of cyclohexanone. Reaction conditions: w (cyclohexanone)/w (catalyst)/w (acetonitrile)/w (benzaldehyde) = 1/0.24/30/2.4; reaction time: 5 h; reaction temperature: 70 °C.

Table 3 Performance of tin-based catalysts in the B-V oxidation of cyclohexanone with molecular oxygen

Catalysts	Cyclohexanone conversion/%	ε-Caprolactone selectivity/%	Reference
MTS-12	97.8	98.2	This work
Sn-Al-7	90.8	91.7	[26]
15Sn-TiO_2	91.4	93.2	[27]
18Sn-TiO_2-EN	94.1	95.2	[28]
Fe-Sn-O mixed oxides	90–99	–	[59]
Mg-Sn-O mixed oxides	87.6	–	[59]
FeTPPCl/SnO2	96.0	> 99	[60]
Co-Sn, Cu-Sn and Ni-Sn	78.5–83.1	85–89	[61]
SnTPP/4A-MS	83	> 99	[62]

the MTS-12 catalyst showed almost the highest cyclohexanone conversion than other tin-based catalysts. Although ε-caprolactone selectivity was lower than that of FeTPPCl/SnO_2 and SnTPP/4A-MS with complicated preparation procedure, the ε-caprolactone yield is slightly higher, which further proved the remarkable catalytic performance and potential application of MTS-12 catalyst.

3.3 Formation mechanism for MTS-x samples

Figure 10 shows possible formation mechanism of MTS-x catalysts. The key points for the synthesis procedure were the hydrolysis and condensation of the two different precursors, where the PVP was as a stabilizer and dispersant to coordinate the hydrolysis rate and prevent the formation of their agglomerates. And then, HDA was introduced as a precipitation accelerator [38] and a morphology control agent by increasing the hydrogen-bonding interactions [41] to promote the formation of spheres. After that, MTS-x catalysts with regular spheres can be obtained followed by self-organization and short range packing. The specific hydrolysis and condensation mechanisms are as follows:

3.3.1 Step 1: Titanium precursor hydrolysis/condensation

$$Ti(OC_4H_9)_4 + xH_2O \rightarrow (OC_4H_9)_{4-x} - Ti - (OH)_x + xC_4H_9OH$$

$$(OC_4H_9)_{4-x}(OH)_{x-1} - Ti - OH + HO - Ti - (OC_4H_9)_{4-x}(OH)_{x-1} \rightarrow (OC_4H_9)_{4-x}(OH)_{x-1} - Ti - O - Ti - (OC_4H_9)_{4-x}(OH)_{x-1} + H_2O$$

$$(OC_4H_9)_{4-x}(OH)_{x-1}Ti - OH + C_4H_9O - Ti - (OC_4H_9)_{3-x}(OH)_x \rightarrow (OC_4H_9)_{4-x}(OH)_{x-1} - Ti - O - Ti - (OC_4H_9)_{3-x}(OH)_x + C_4H_9OH$$

Titanium complexes with some hydroxyl groups were formed by the hydrolysis of tetrabutyl titanate, and Ti-O-Ti bonds would be further produced by the condensation between two or more of the titanium complexes [63, 64].

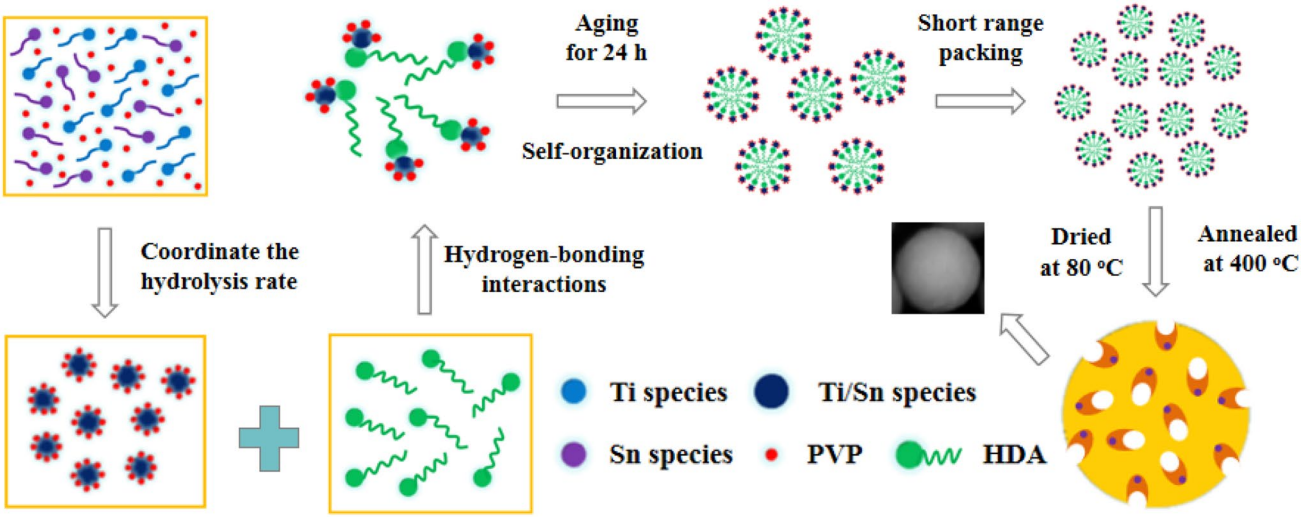

Fig. 10 Preparation mechanism of MTS-x catalysts

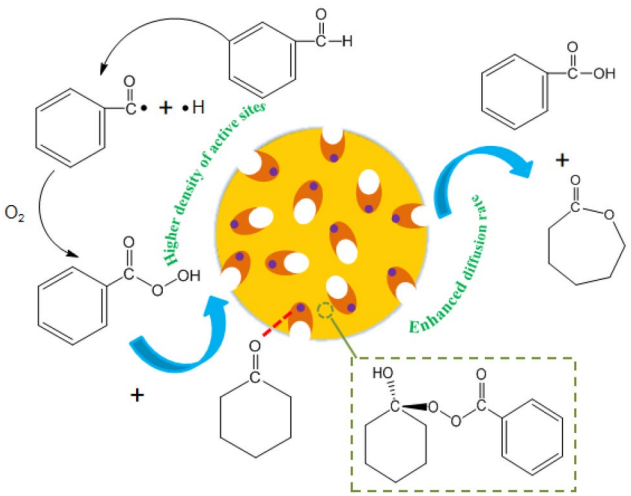

Fig. 11 Reaction pathway for the MTS-x catalysts

3.3.2 Step 2: Tin precursor hydrolysis/condensation

$$SnCl_4 + C_2H_5OH \rightarrow Sn(C_2H_5O)_4 + 4HCl$$

$$Sn(C_2H_5O)_4 + xH_2O \rightarrow (OC_2H_5)_{4-x} - Sn - (OH)_x + xC_2H_5OH$$

$$(OC_2H_5)_{4-x}(OH)_{x-1} - Sn - OH + HO - Sn - (OC_2H_5)_{4-x}(OH)_x \rightarrow (OC_2H_5)_{4-x}(OH)_{x-1} - Sn - O - Sn - (OC_2H_5)_{4-x}(OH)_{x-1} + H_2O$$

$$(OC_2H_5)_{4-x}(OH)_{x-1} - Sn - OH + C_2H_5O - Sn(OC_2H_5)_{3-x}(OH)_x \rightarrow (OC_2H_5)_{4-x}(OH)_{x-1} - Sn - O - Sn - (OC_2H_5)_{3-x}(OH)_x + C_2H_5OH$$

The hydrolysis and condensation procedure of tin precursor is similar as the titanium precursor besides that the tin tetrachloride is firstly alcoholized by the reaction with ethanol.

3.3.3 Step 3: Titanium and tin complexes condensation

$$(OC_4H_9)_{4-x}(OH)_{x-1} - Ti - OH + HO - Sn - (OC_2H_5)_{4-x}(OH)_{x-1} \rightarrow (OC_4H_9)_{4-x}(OH)_{x-1} - Ti - O - Sn - (OC_2H_5)_{4-x}(OH)_{x-1} + H_2O$$

$$(OC_4H_9)_{4-x}(OH)_{x-1} - Ti - OH + C_2H_5O - Sn - (OC_2H_5)_{3-x}(OH)_x \rightarrow (OC_4H_9)_{4-x}(OH)_{x-1} - Ti - O - Sn - (OC_2H_5)_{3-x}(OH)x + C_2H_5OH$$

At the same time, Ti-O-Sn bonds would be gradually formed by the condensation of titanium and tin complexes.

In order to promote the formation of the bonding network, HDA was added in the preparation system to accelerate the hydrolysis and condensation rates [65] and the PVP was also introduced to modulate the formation process of the microspheres.

3.4 Reaction pathway for the MTS-x catalysts

Figure 11 shows reaction pathway for the MTS-x catalysts. Firstly, benzaldehyde decomposes into benzoyl and hydrogen radicals, and then the benzoperoxy acid was formed by the combination with molecular oxygen. The activated cyclohexanone with the Lewis acidities was attacked by the generated benzoperoxyacid as a nucleophile to generate a "Criegee" intermediate. The product of ε-caprolactone was obtained by the B–V rearrangement of the "Criegee" intermediate, while the by-product of benzoic acid was also formed. The higher density of active sites with Lewis acidities and shorter diffusion channels would act as the key reasons for the higher catalytic performance of the MTS-x catalysts.

4 Conclusions

In this paper, a series of mesoporous MTS-x catalyst with specific microspheres were first successfully synthesized by a PVP-assisted sol-gel method. The characterization results showed that the introduction of tin species into the framework of TiO_2 microspheres not only increased the pore volume and specific surface area, but also increased the strength of Lewis acidity. The PVP and HDA would act as different roles in the formation of regular microspheres, which is essential to acquisition of the higher catalytic performance in the B–V oxidation of cyclohexanone with molecular oxygen. When the weight percent of tin to titanium species was 12, the MTS-12 catalyst would be the best candidate with no obvious loss of catalytic performance even after repeated use for 5 times.

Acknowledgements This work was supported by the National Key Research and Development Program of China (No. 2019YFD1101204); University-Industry Cooperation Projects of Jiangsu Province (No. BY20200011) and Open Project of Beijing Key Laboratory for Enze Biomass and Fine Chemicals.

Declarations

Conflict of Interest The authors declare no conflict of interest.

References

1. G. Strukul, Transition metal catalysis in the baeyer-villiger oxidation of ketones[J]. Angewandte Chemie Int. Ed. **37**(9), 1198–1209 (1998)
2. G.-J. ten Brink, I.W.C.E. Arends, R.A. Sheldon, The Baeyer-villiger reaction: new developments toward greener procedures[J]. Chem. Rev. **104**(9), 4105–4123 (2004)
3. R.A. Michelin, P. Sgarbossa, A. Scarso, G. Strukul, The baeyer-villiger oxidation of ketones: a paradigm for the role of soft lewis acidity in homogeneous catalysis[J]. Coord. Chem. Rev. **254**(5–6), 646–660 (2010)
4. K. Kaneda, T. Yamashita, Heterogeneous baeyer-villiger oxidation of ketones using m-chloroperbenzoic acid catalyzed by hydrotalcites[J]. Tetrahedr. Lett. **37**(26), 4555–4558 (1996)
5. B. Schweitzer-Chaput, T. Kurtén, M. Klussmann, Acid-mediated formation of radicals or baeyer-villiger oxidation from criegee adducts[J]. Angewandte Chemie **54**(40), 11848–11851 (2015)
6. Z. Zhu, H. Xu, J. Jiang, X. Liu, J. Ding, P. Wu, Postsynthesis of FAU-type stannosilicate as efficient heterogeneous catalyst for baeyer-villiger oxidation[J]. Appl. Catal. A General **519**, 155–164 (2016)
7. A. Sinhamahapatra, A. Sinha, S.K. Pahari, N. Sutradhar, H.C. Bajaj, A.B. Panda, Room temperature baeyer-villiger oxidation using molecular oxygen over mesoporous zirconium phosphate[J]. Catal. Sci. Technol. **2**(11), 2375–2382 (2012)
8. W. Zheng, R. Tan, X. Luo, C. Xing, D. Yin, SnO_2 Nanoparticle-decorated graphene oxide sheets efficiently catalyze baeyer-villiger oxidation with H_2O_2[J]. Catal. Lett. **146**(2), 281–290 (2016)
9. G.-J. ten Brink, J.-M. Vis, I.W.C.E. Arends, R.A. Sheldon, Selenium-catalyzed oxidations with aqueous hydrogen peroxide. 2. baeyer-villiger reactions in homogeneous solution[J]. J. Org. Chem. **66**(7), 2429–33 (2001)
10. Y. Tohru, T. Katsuya, K. Koji, T. Toshihiro, I. Satoshi, M. Teruaki, The baeyer-villiger oxidation of ketones catalyzed by nickel(ii) complexes with combined use of molecular oxygen and aldehyde[J]. Chem. Lett. **4**(4), 641–644 (1991)
11. T. Yamada, T. Takai, O. Rhode, T. Mukaiyama, Direct epoxidation of olefins catalyzed by nickel(II) complexes with molecular oxygen and aldehydes[J]. Bull. Chem. Soc. Japan **64**(7), 2109–2117 (1991)
12. C. Jimenez-Sanchidrian, J.R. Ruiz, ChemInform abstract: the baeyer-villiger reaction on heterogeneous catalysts[J]. Tetrahedron **64**(9), 2011–2026 (2008)
13. K. Mandai, M. Hanata, K. Mitsudo, H. Mandai, S. Suga, H. Hashimoto, J. Takada, Bacteriogenic iron oxide as an effective catalyst for baeyer-villiger oxidation with molecular oxygen and benzaldehyde[J]. Tetrahedron **71**(50), 9403–9407 (2015)
14. X.Y. Zhang, H.L. Yang, G.X. Yang, S.W. Li, X. Wang, J.T. Ma, Metal-free mesoporous SiO_2 nanorods as a highly efficient catalyst for the baeyer-villiger oxidation under mild conditions[J]. ACS Sustain. Chem. Eng. **6**(5), 5868–5876 (2018)
15. J. Zang, Y.J. Ding, Y.P. Pei, R.H. Lin, T. Liu, L. Yan, Y. Lu, Efficient Co_3O_4/SiO_2 catalyst for the Baeyer-Villiger oxidation of cyclohexanone[J]. React. Kinet. Mech. Catal. **112**(1), 159–171 (2014)
16. Y.L. Ma, Z.Y. Liang, S.X. Feng, Y.D. Zhang, Baeyer-villiger oxidation of cyclohexanone by molecular oxygen with Fe-Sn-O mixed oxides as catalysts[J]. Appl. Organometall. Chem. **29**(7), 450–455 (2015)
17. C. Jimenez-Sanchidrian, J.M. Hidalgo, R. Llamas, J.R. Ruiz, Baeyer-villiger oxidation of cyclohexanone with hydrogen peroxide/benzonitrile over hydrotalcites as catalysts[J]. Appl. Catal. A: General **312**(8), 86–94 (2006)
18. H. Subramanian, E.G. Nettleton, S. Budhi, R.T. Koodali, Baeyer-villiger oxidation of cyclic ketones using Fe containing MCM-48 cubic mesoporous materials[J]. J. Mol. Catal. A Chem. **330**(1–2), 66–72 (2010)
19. Y. Nabae, H. Rokubuichi, M. Mikuni, Y. Kuang, T. Hayakawa, M. Kakimoto, Catalysis by carbon materials for the aerobic baeyer-villiger oxidation in the presence of aldehydes[J]. ACS Catal. **3**(2), 230–236 (2013)
20. G. Liu, L. Sun, W. Luo, Y. Yang, J.H. Liu, F. Wang, C.J. Guild, Aerobic baeyer-villiger oxidation of ketones over mesoporous Mn-Ce and Mn-Co composite oxides in the presence of benzaldehyde: the effect of valence state[J]. Mol. Catal. **458**, 9–18 (2018)
21. Z.W. Zhou, J.Z. Wang, J. Qin, Y. Yu, W.L. Wu, The Multifunctional mesoporous Sn-Cu-Ti catalysts for the B-V oxidation of cyclohexanone by molecular oxygen[J]. J. Porous Mater. **25**(3), 835–843 (2018)
22. A. Corma, L.T. Nemeth, M. Renz, S. Valencia, Sn-zeolite beta as a heterogeneous chemoselective catalyst for baeyer-villiger oxidations[J]. Nature **412**(6845), 423 (2001)
23. A. Corma, M.T. Navarro, L. Nemeth, M. Renz, Sn-MCM-41—a heterogeneous selective catalyst for the baeyer-villiger oxidation with hydrogen peroxide[J]. Chem. Commun. **21**, 2190–2191 (2001)
24. T. Chen, B.D. Wang, Y.C. Li, L. Liu, S.F. Qiu, Hydrothermal synthesis of tin containing mesoporous silicas and their catalytic performance over baeyer-villiger oxidation of cyclohexanone to ε-caprolactone: comparison of Sn/MCM-41 and Sn/SBA-15[J]. J. Porous Mater. **22**(4), 949–957 (2015)
25. R. Maheswari, M.P. Pachamuthu, A. Ramanathan, B. Subramaniam, Synthesis, characterization, and epoxidation activity of tungsten-incorporated SBA-16 (W-SBA-16)[J]. Indus. Eng. Chem. Res. **53**(49), 18833–18839 (2014)
26. Z.W. Zhou, P.C. Yu, J. Qin, W.L. Wu, L. Xu, Z.Q. Gu, X.Q. Liu, Synthesis, characterization and catalytic performance of ordered mesoporous Sn-Al catalysts[J]. J. Porous Mater. **23**(1), 239–245 (2016)
27. Z.W. Zhou, Y. Yu, P.C. Yu, J. Qin, S.S. Dai, W.L. Wu, Ordered mesoporous Sn-TiO_2 catalysts via an evaporation induced self-assembly method for the baeyer-villiger oxidation of cyclohexanone by molecular oxygen[J]. React. Kinet. Mech. Catal. **120**(1), 295–305 (2017)
28. Z.R. Liu, Z.W. Zhou, J. Qin, G. Liu, H. Huang, W.L. Wu, Mesoporous Sn-TiO_2 catalysts by molecular protection strategy for the baeyer-villiger oxidation of cyclohexanone with molecular oxygen[J]. Chemistryselect **3**(23), 6434–6439 (2018)
29. P.P. Qiu, B. Ma, C.T. Hung, W.L.D.Y. Zhao, Spherical mesoporous materials from single to multilevel architectures[J]. Acc. Chem. Res. **52**(10), 2928–2938 (2019)
30. J.H. Pan, Q. Wang, D.W. Bahnemann, Hydrous TiO_2 spheres: an excellent platform for the rational design of mesoporous anatase spheres for photoelectrochemical applications[J]. Catal. Today **230**(7), 197–204 (2014)
31. X. Jiang, T. Herricks, Y. Xia, Monodispersed spherical colloids of titania: synthesis, characterization, and crystallization[J]. Adv. Mater. **15**(14), 1205–1209 (2003)
32. W.Y. Cheng, J.R. Deka, Y.C. Chiang, A. Rogeau, S.Y. Lu, One-Step, surfactant-free hydrothermal method for syntheses of mesoporous TiO_2 nanoparticle aggregates and their applications in high efficiency dye-sensitized solar cells[J]. Chem. Mater. **24**(16), 3255–3262 (2012)
33. T. Kamegawa, Y. Ishiguro, H. Seto, H. Yamashita, Enhanced photocatalytic properties of TiO_2-loaded porous silica with hierarchical macroporous and mesoporous architectures in water purification[J]. J. Mater. Chem. A **3**(5), 2323–2330 (2015)
34. Q. Yue, J. Li, Y. Zhang, X. Cheng, X. Chen, P. Pan, J. Su, A.A. Elzatahry, A. Alghamdi, Y. Deng, D. Zhao, Plasmolysis-inspired nanoengineering of functional yolk-shell microspheres with magnetic core and mesoporous silica shell[J]. J. Am. Chem. Soc. **139**(43), 15486–15493 (2017)
35. C. Wang, F. Wang, Y. Zhao, Y. Li, Q. Yue, Y. Liu, A.A. Elzatahry, A. Al-Enizi, Y. Wu, Y. Deng, D. Zhao, Hollow TiO_{2-x} porous microspheres composed of well-crystalline nanocrystals for

high-performance lithium-ion batteries[J]. Nano Res. **9**(1), 165–173 (2016)
36. Y. Yamaguchi, T. Shimodo, S. Usuki, K. Torigoe, C. Terashima, K. Katsumata, M. Ikekita, A. Fujishima, H. Sakai, K. Nakata, Different hollow and spherical TiO_2 morphologies have distinct activities for the photocatalytic inactivation of chemical and biological agents[J]. Photochem. Photobiol. Sci. **15**(8), 988–994 (2016)
37. M. Pal, L. Wan, Y. Zhu, Y. Liu, Y. Liu, W. Gao, Y. Li, G. Zheng, A.A. Elzatahry, A. Alghamdi, Y. Deng, D. Zhao, Scalable synthesis of mesoporous titania microspheres via spray-drying method[J]. J. Colloid Interface Sci. **479**, 150–159 (2016)
38. Y. Ding, I.S. Yang, C.Z. Li, X. Xia, W.I. Lee, S.Y. Dai, Detlef W. Bahenmann, J.H. Pan. Nanoporous TiO_2 Spheres with Tailored Textural Properties: Controllable Synthesis, Formation Mechanism, and Photochemical Applications[J]. Progress in Materials Science, 2020, 109.
39. Y.A. Kumar, K.D. Kumar, H.J. Kim, A novel electrode for supercapacitors: efficient pvp-assisted synthesis of Ni_3S_2 nanostructures grown on ni foam for energy storage[J]. Dalton Transact. **49**(19), 4050–4059 (2020)
40. J.C. Shu, M.S. Cao, M. Zhang, X.X. Wang, W.Q. Cao, X.Y. Fang, M.Q. Cao, Molecular patching engineering to drive energy conversion as efficient and environment-friendly cell toward wireless power transmission[J]. Adv. Funct. Mater. **30**(10), 1908299 (2020)
41. X.S. Guo, Y.L. Chen, M. Su, D. Li, G.C. Li, C.D. Li, Y. Tian, C.C. Hao, Q.Q. Lei, Enhanced electrorheological performance of Nb-Doped TiO_2 microspheres based suspensions and their behavior characteristics in low-frequency dielectric spectroscopy[J]. ACS Appl. Mater. Interfaces **7**(48), 26624–26632 (2015)
42. W.G. Liu, Y.M. Xu, W. Zhou, X.F. Zhang, X.L. Cheng, H. Zhao, S. Dao, L.H. Huo, A facile synthesis of hierarchically porous TiO_2 microspheres with carbonaceous species for visible-light photocatalysis[J]. J. Mater. Sci. Technol. **33**(1), 39–46 (2016)
43. A. Yasin, F.Q. Guo, G.P. Demopoulos, Aqueous, screen-printable paste for fabrication of mesoporous composite anatase-rutile TiO_2 nanoparticle thin films for (Photo) electrochemical devices[J]. ACS Sustain. Chem. Eng. **4**(4), 2173–2181 (2016)
44. X.D. Zhu, L.X. Pei, R.R. Zhu, J. Yu, R.Y. Tang, F. Wei, Preparation and characterization of Sn/La co-doped TiO_2 nanomaterials and their phase transformation and photocatalytic activity[J]. Sci. Rep. **8**(1), 12387–12401 (2018)
45. M.E. Yu, C.T. Li, G.M. Zeng, Y. Zhou, X.N. Zhang, Y.E. Xie, The selective catalytic reduction of NO with NH_3 over a novel Ce-Sn-Ti mixed oxides catalyst: promotional effect of SnO_2[J]. Appl. Surf. Sci. **342**, 174–182 (2015)
46. M. Nikoorazm, N. Noori, B. Tahmasbi, A palladium complex immobilized onto mesoporous silica: a highly efficient and reusable catalytic system for carbon-carbon bond formation and anilines synthesis[J]. Trans. Metal Chem. **42**(5), 469–481 (2017)
47. H.Y. Li, D.J. Wang, P. Wang, H.M. Fan, T.F. Xie, Synthesis and studies of the visible-light photocatalytic properties of near-monodisperse Bi-doped TiO_2 nanospheres[J]. Chem.-A Eur. J. **15**(45), 12521–12527 (2009)
48. Q. Zhang, H. Yang, Y. Wei, Effect of ethanol on the crystallinity and acid sites of MFI zeolite nanosheets[J]. RSC Adv. **4**(100), 56938–56944 (2014)
49. M.P. Pachamuthu, K. Shanthi, R. Luque, A. Ramanathan, Identification of potential therapeutics to conquer drug resistance in salmonella typhimurium: drug repurposing strategy[J]. Green Chem. **15**(8), 2158–2166 (2013)
50. G.H. Chen, S.Z. Ji, Y.H. Sang, S. Chang, Y. Wang, P. Hao, J. Claverie, H. Liu, G. Yu, Synthesis of scaly Sn_3O_4/TiO_2 nanobelt heterostructures for enhanced uv-visible light photocatalytic activity[J]. Nanoscale **7**(7), 3117–3125 (2015)
51. W.J. Hong, M. Kang, The super-hydrophilicities of Bi-TiO_2, V-TiO_2, and Bi-V-TiO_2 nano-sized particles and their benzene photodecompositions with H_2O addition[J]. Mater. Lett. **60**(9–10), 1296–1305 (2006)
52. Y. Xie, X. Zhao, H. Tao, The Influence of O_2 partial pressure on the structure and surface wettability of C-modified TiO_2 films prepared by magnetron co-sputtering[J]. Chem. Phys. Lett. **457**(1–3), 148–153 (2008)
53. I. Mahdi, B. Susanta, K. Se-Hun, Influence of surface defects and size on photochemical properties of SnO_2 nanoparticles[J]. Materials **11**(6), 904 (2018)
54. X. Zhang, Z.Q. Bao, X.Y. Tao, H.X. Sun, W. Chen, X.F. Zhou, Sn-doped TiO_2 nanorod arrays and application in perovskite solar cells[J]. RSC Adv. **4**(109), 64001–64005 (2014)
55. Y. Masuda, T. Ohji, K. Kato, Multineedle TiO_2 nanostructures, self-assembled surface coatings, and their novel properties[J]. Crys. Design **10**(2), 913–822 (2010)
56. Z.Q. Li, Y.P. Que, L.E. Mo, W.C. Chen, Y. Ding, Y.M. Ma, L. Jiang, L.H. Hu, S.Y. Dai, One-pot synthesis of mesoporous TiO_2 micropheres and its application for high-efficiency dye-sensitized solar cells[J]. ACS Appl. Mater. Interfaces **7**(20), 10928–10934 (2015)
57. J. Andas, F. Adam, I.A. Rahman, T.Y. Yun, Optimization and mechanistic study of the liquid-phase oxidation of naphthalene over biomass-derived iron catalyst[J]. Chem. Eng. J. **252**(1), 382–392 (2014)
58. J.S. Reddy, P. Liu, A. Sayari, Vanadium containing crystalline mesoporous molecular sieves Leaching of vanadium in liquid phase reactions[J]. Appl. Catal. A General **148**(1), 7–21 (1996)
59. Y.L. Ma, Z.Y. Liang, S.X. Feng, B-V oxidation of cyclohexanone by molecular oxygen with Fe-Sn-O mixed oxides as catalysts[J]. Appl. Organometal. Chem. **29**, 450–455 (2015)
60. S.Y. Chen, X.T. Zhou, Y. Li, R.C. Luo, H.B. Ji, Biomimetic Baeyer-Villiger oxidation of ketones with SnO_2 as cocatalyst, features in activating carbonyl group of substrates[J]. Chem. Eng. J. **241**, 138–144 (2014)
61. S. Hazra, N.M.R. Martins, M.L. Kuznetsov, M.F.C. Guedes da Silva, A.J.L. Pombeiro, Flexibility and lability of a phenyl ligand in heteroorganometallic 3d metal-Sn(IV) compounds and their catalytic activity in Baeyer-Villiger oxidation of cyclohexanone[J]. Dalton Trans. **46**(39), 13364–13375 (2019)
62. S.Y. Chen, X.T. Zhou, H.B. Ji, Insight into the cocatalyst effect of 4A molecular sieve on Sn(II) porphyrin-catalyzed B-V oxidation of cyclohexanone[J]. Catal. Today **264**, 191–197 (2016)
63. D.P. Cozzoli, A. Kornowski, H. Weller, Low-temperature synthesis of soluble and processable organic-capped anatase TiO_2 nanorods[J]. J. Am. Chemi. Soc. **125**(47), 14539–14548 (2003)
64. X.C. Jiang, T. Herricks, Y.N. Xia, Monodispersed spherical colloids of titania: synthesis, characterization, and crystallization[J]. Adv. Mater. **15**(14), 1205–1209 (2010)
65. J.G. Yu, J.J. Fan, L. Zhao, Dye-sensitized solar cells based on hollow anatase TiO_2 spheres prepared by self-transformation method[J]. Electrochimica Acta **55**(3), 597–602 (2010)